Available online at www.sciencedirect.com
SCIENCE DIRECT®
Journal of Power Sources 137 (2004) 105–110
JOURNAL OF POWER SOURCES
www.elsevier.com/locate/jpowsour

Short communication

Studies on capacity increase of $Li_{1.27}Cr_{0.2}Mn_{0.53}O_2$-based lithium batteries

Xianglan Wu*, Soon Ho Chang, Yong Joon Park, Kwang Sun Ryu

Basic Research Laboratory, Electronics and Telecommunications Research Institute, 161 Gajeong-dong, Yuseong-gu, Daejeon 305-350, South Korea

Received 18 February 2004; accepted 23 May 2004
Available online 31 July 2004

Abstract

A $Li/Li_{1.27}Cr_{0.2}Mn_{0.53}O_2$ cell is found to deliver an excellent discharge capacity of around 260 mAh g^{-1}, but exhibits a continuous increase in capacity on extended cycling. To explain this latter behaviour, various electrochemical measurements and ex situ X-ray diffraction (XRD) are performed. Both cyclic voltammetry and ex situ XRD reveal that an accumulation of transition metal atoms (Cr or Mn) in the lithium layer with cycling results in a monoclinic phase and capacity increase. Studies using ac impedance spectroscopy reveal that the structural change mainly occurs during the charging process.

Keywords: Lithium batteries; Capacity increase; Chromium accumulation; Impedance spectra

1. Introduction

Recently, $Li[Cr_xLi_{(1/3-x/3)}Mn_{(2/3-2x/3)}]O_2$ with α-$NaFeO_2$ structure was reported to exhibit excellent cycling retention though there was a large irreversible capacity on the first cycle [1–5]. Two research groups [6,7] have identified the origin of the irreversible capacity through EXAFS and in situ X-ray diffraction (XRD). Except for the large irreversible capacity at the first cycle, we have found that $Li_{1.27}Cr_{0.2}Mn_{0.53}O_2$ ($x = 0.2$) material displays continuous increase in capacity on extended cycling [8]. A similar result has been observed for $Li/Li[Cr_xLi_{(1/3-x/3)}Mn(_{2/3-2x/3})]O_2$ ($x = 1/3$, 1/4) materials [4]. $Li(Li_{0.17}Ni_{0.25}Mn_{0.58})O_2$ material with the same layer structure has also been reported to deliver increased capacity with cycling, and this was attributed primarily to the differential capacity peak developed at 3.2 V on charging [9]. Considering the lack of an overall description of the capacity increase and possible future application of such materials in Li-ion cells, it is important to understand the electrochemical behaviour and structural change of $Li_{1.27}Cr_{0.2}Mn_{0.53}O_2$ on extended cycles.

The change in the capacity of a lithium battery during cycling may be associated with certain unwanted side-reactions. These reactions have been reported to result in electrolyte decomposition, passive film formation, active material dissolution, and phase changes in the electrode material [10]. It has been further shown that there is a strong effect on the electroanalytical response of the electrode when a destructive side-reaction occurs and leads to capacity change [11]. Therefore, both slow-scan cyclic voltammetry and impedance spectroscopy are very good measures of stable behaviour of a reversible electrode. To shed light on the capacity increase of $Li_{1.27}Cr_{0.2}Mn_{0.53}O_2$ electrode on extended cycling; we have investigated the electrode using ex situ X-ray diffractometry and electroanalytical techniques.

2. Experimental

Layered $Li_{1.27}Cr_{0.2}Mn_{0.53}O_2$ was prepared from a mixture of manganese acetate, chromium acetate and lithium hydroxide using a solution method [8]. A solution of LiOH was added to a pre-dissolved solution of manganese acetate and chromium acetate with stirring. The mixed precipitation solution was heated on a hot plate until it became viscous. Then, it was coated on a titanium foil and heated on a hot plate to give porous powders. The powders were fired at 700 °C for 3 h and then calcined at 900 °C for 12 h in air. This was followed by a quenching procedure to room temperature. X-ray diffraction measurements were conducted on a Philips PW3040/60 X'pert PRO diffractometer using Cu Kα

* Corresponding author. Tel.: +82 42 860 6891; fax: +82 42 860 6836.
E-mail address: wxlpostech@yahoo.com (X. Wu).

0378-7753/$ – see front matter © 2004 Elsevier B.V. All rights reserved.
doi:10.1016/j.jpowsour.2004.05.043

radiation. To perform ex situ diffraction studies, cells using $Li_{1.27}Cr_{0.2}Mn_{0.53}O_2$ electrodes were charged or discharged to the targeted voltage. Then, the cells were disassembled in a dry room and the positive electrode was washed with dimethylcarbonate solvent to remove the dissolved salt and residual ethylene carbonate (EC) of the electrolyte.

Electrochemical measurements were carried out using pouch-type cells that each comprised a lithium metal foil anode, a separator, and a cathode. The cathodes were prepared by mixing $Li_{1.27}Cr_{0.2}Mn_{0.53}O_2$ powder, super P black (MMM carbon Co.) and poly(vinylidene)fluoride (PVDF) binder in a ratio of 85:7.5:7.5 by weight. The mixture was made into a slurry in *N*-methyl-2-pyrrolidone (NMP) solution and cast as a film on an aluminum foil using a doctor blade. The cast was dried at 130 °C for 12 h in vacuum and pressed to an appropriate thickness in a roll press. The electrolyte was 1 M $LiPF_6$ dissolved in 1:1 ethylene carbonate and dimethyl carbonate (DMC). The cells were cycled galvanostatically over a potential range of 2.0–4.9 V using a Maccor Battery Tester System. Cyclic voltammograms were obtained at a scan rate of 0.05 mV s^{-1} over a potential range of 2.0–4.9 V versus a Li/Li^+ reference electrode. Impedance experiments were performed on $Li_{1.27}Cr_{0.2}Mn_{0.53}O_2$ electrodes that were at different states of change and discharge. The data were collected in the frequency range 0.1 Hz to 100 kHz with an ac voltage signal of ±5 mV.

3. Results and discussion

Charge–discharge curves for a $Li_{1.27}Cr_{0.2}Mn_{0.53}O_2$ cell at different cycles are compared in Fig. 1. The cell delivered a capacity of 257 mAh g^{-1} with a sloping voltage line on the first discharge, and maintained the capacity for at least 20 cycles though the sloping line gradually shifted to a slightly lower voltage. The downward shift of discharge

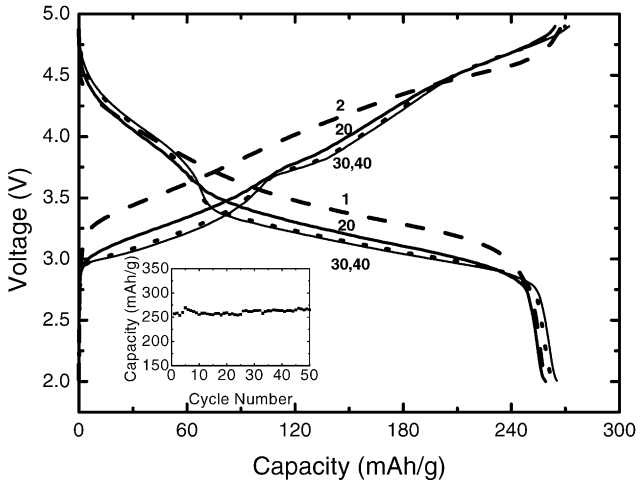

Fig. 1. Charge and discharge curves for $Li/Li_{1.27}Cr_{0.2}Mn_{0.53}O_2$ cell at different cycles. Data were collected at current density of 12 mA g^{-1} over voltage range 2.0–4.9 V.

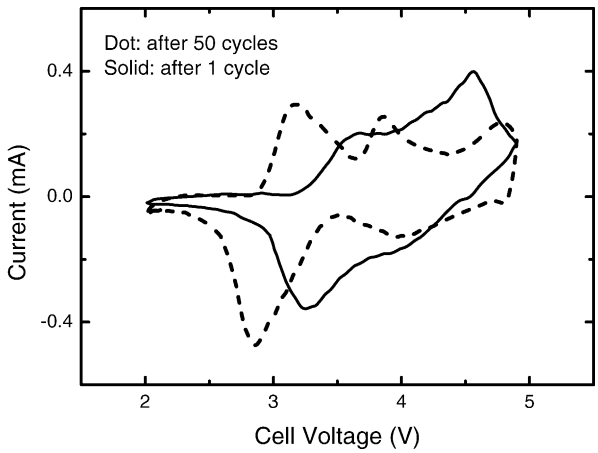

Fig. 2. Cyclic voltammograms for $Li/Li_{1.27}Cr_{0.2}Mn_{0.53}O_2$ cell obtained at scan rate of 0.05 mV s^{-1}.

voltage may be attributed to a change in the electrode material structure. With continued cycling, the cell delivers a slightly increased capacity, i.e. around 264 mAh g^{-1} from 25th cycle as shown in the inset, and the sloping line splits into two due to a more severe change in the structure. Furthermore, the polarization between charge and discharge decreases with cycling until 30th cycle and beyond that both the capacity and voltage profiles are relatively stable. These results reveal that a $Li/Li_{1.27}Cr_{0.2}Mn_{0.53}O_2$ cell shows remarkable cycling stability at room temperature, despite the difference in the voltage profiles, during extended cycling. On the other hand, there is no plateau at around 2.9 V on extended cycling, which suggests that material does not transform into a spinel configuration [12].

The voltammetric behaviour of $Li_{1.27}Cr_{0.2}Mn_{0.53}O_2$ electrodes after 1 and 50 cycles is shown in Fig. 2. It is clear that the profile of the second cycle is different from that of the 50th cycle. The anodic peak at around 3.7 V shifts to a more negative potential of 3.2 V, while the peak at 4.6 V splits into 3.9 and 4.8 V peaks at the 50th cycle, respectively. There is, however, no evolution of two typical spinel peaks between 4.0 and 4.3 V [13,14]. This reinforces the above conclusion that the material does not transform into a spinel structure with cycling. Similarly, the broad cathodic peak at 3.3 V is clearly separated into 2.9 and 4.0 V peaks and increases in intensity at the 50th cycle. In short, the small peaks around 4.0 and 4.8 V may be related to the redox couple Cr^{4+}/Cr^{6+} and its redistribution in the Li layer, as in the case of undoped $LiMn_2O_4$, while the large peaks around 3.0 V correspond to the redox couple Cr^{3+}/Cr^{4+} [15–18]. To further conform the structural change with cycling, we have carried out ex situ XRD studies.

The ex situ X-ray diffraction patterns of $Li_{1.27}Cr_{0.2}Mn_{0.53}O_2$ electrodes on the first cycle are shown in Fig. 3. Comparing Fig. 1(b) with (a), it is clear that the intensity of the (0 1 2) peak is increased intensively. The difference may be attributed to the aluminum foil. Other peaks, except for (1 0 4), shift smoothly but do not change significantly during

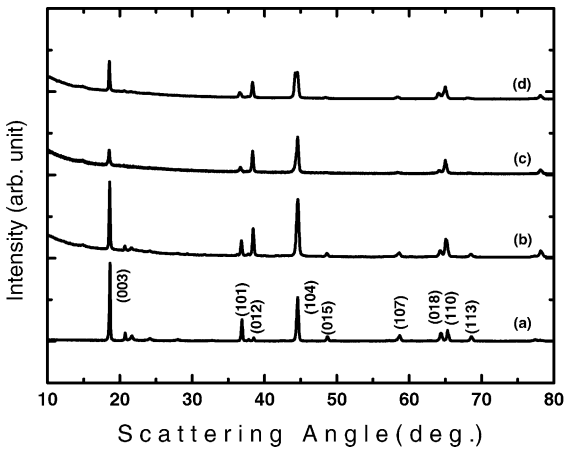

Fig. 3. X-ray diffraction patterns for $Li_{1.27}Cr_{0.2}Mn_{0.53}O_2$ electrodes: (a) powder, (b) pristine, (c) after first charge, (d) after first discharge.

Table 1
Unit cell parameters for $Li_{1.27}Cr_{0.2}Mn_{0.53}O_2$

State	a (Å)	c (Å)	c/a
Powder sample	2.854	14.264	4.998
Pristine electrode	2.859	14.273	4.991
After first charge	2.862	14.308	4.999
After first discharge	2.873	14.328	4.987

the first cycle. This suggests that the electrode material maintains a layered structure throughout the charge–discharge process. This is further confirmed by the lattice parameter data ($c/a = 4.99$) in Table 1. As for the (1 0 4) peak in Fig. 1(d), there are two split lines at the top due to the co-existence of a small monoclinic phase [9].

Fig. 4 compares the ex situ X-ray diffraction patterns of $Li_{1.27}Cr_{0.2}Mn_{0.53}O_2$ electrodes measured at different states of discharge. There is a shoulder on the left side of the (1 0 4) peak when the $Li/Li_{1.27}Cr_{0.2}Mn_{0.53}O_2$ cell is discharged to 3.4 V, which indicates the start of structure change. After the end of first discharge, the shoulder peak increases in intensity and eventually results in split of the (1 0 4) peak, though the separation is not obvious. This suggests that the structural change has not reached completion. With continued cycling, the shoulder peak shifts downwards slowly to a lower angle and separates well at the end of the 30th discharge. This is in good accordance with the charge–discharge curves that show two distinct plateaus in Fig. 1. On the other hand, it has been reported that, during the charge process, Cr or Mn atoms in $Li[Cr_xLi_{(1/3-x/3)}Mn_{(2/3-2x/3)}]O_2$ ($x = 1/3$) migrate from their original octahedral sites in the transition metal layer to neighbour tetrahedral sites in the lithium layer and then further to octahedral sites in the same lithium layer. Though many of the migrated transition metal atoms returned to their original octahedral sites in the transition metal layer upon discharge, some amount of transition metal atoms remain on both the tetrahedral and the octahedral sites in lithium layer [6,7]. These residual transition metal atoms induce structural ordering and a large irreversible capacity on the first cycle. Since $Li_{1.27}Cr_{0.2}Mn_{0.53}O_2$ exhibits the same type of irreversible capacity on the first cycle, it is obvious that there are residual Cr or Mn atoms in the lithium layer after discharge [8]. With continued cycling, the amount of residual transition metal atoms in different sites of the lithium layer increases and eventually results in a monoclinic peak on the left side of the (1 0 4) peak. By contrast, the (1 0 4) peak in the previously reported $Li[Cr_xLi_{(1/3-x/3)}Mn_{(2/3-2x/3)}]O_2$ ($x = 1/3$) electrode after first discharge does not show any split [7]. The difference may be attributed to the fact that $Li[Cr_xLi_{(1/3-x/3)}Mn_{(2/3-2x/3)}]O_2$ ($x = 1/3$) material has less pronounced superlattice ordering than $Li_{1.27}Cr_{0.2}Mn_{0.53}O_2$ material.

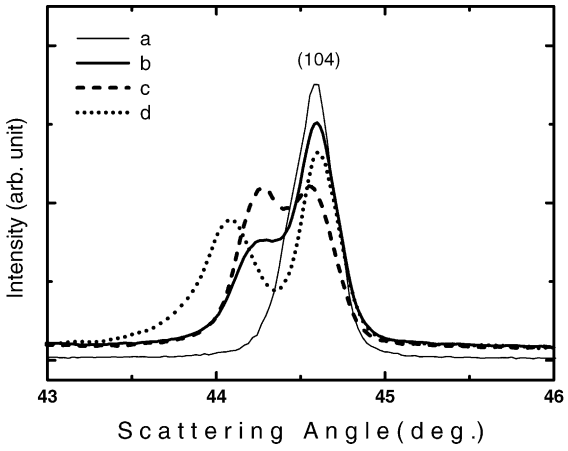

Fig. 4. X-ray diffraction patterns for $Li_{1.27}Cr_{0.2}Mn_{0.53}O_2$ electrodes at selected range: (a) pristine, (b) after discharged to 3.4 V, (c) after first discharge, (d) after 30th discharge.

Nyquist plots of a $Li_{1.27}Cr_{0.2}Mn_{0.53}O_2$ electrode obtained at different states of charge are presented in Fig. 5. The depressed semicircle of each plot can be associated with the electrode surface layer and the charge-transfer process. Similar to $LiNiO_2$, the semicircle is strongly dependent on the potential and is minimal at around 4.15 V [11,19]. On the other hand, the impedance of both fully lithiated and delithiated electrodes reflects resistive electrodes. The data were analyzed using the equivalent circuit shown in Fig. 5. R_{sl} represents the ion-transfer resistance, C_{sl} is the surface-layer capacitance, R_{ct} is the charge-transfer resistance, C_{dl} is the double-layer capacitance, and Z_w is the Warburg impedance. The behaviour of both the surface-layer resistance and the charge-transfer resistance as a function of charge potential is demonstrated in Fig. 6(a). The observed increase in R_{sl} is due to the slow growth of the passive film as a function of time. It is clear that the film grows rapidly below 4.1 V and, thereafter, grows slowly. By contrast, the charge-transfer resistance decreases rapidly with the increase in charge voltage upto 4.15 V, then it experiences a moderate increase with further increase in charge voltage. This may be attributed to a change in interlayer distance that results in easy transfer of lithium ions in the interlayer when it is expanded, and

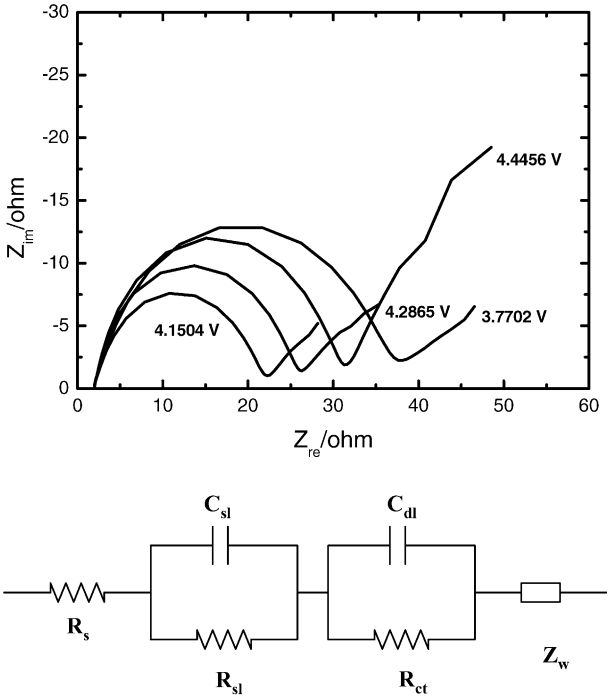

Fig. 5. Nyquist plots for $Li_{1.27}Cr_{0.2}Mn_{0.53}O_2$ electrode measured at different states of charge and the corresponding equivalent circuit.

vice versa. Similar results have been reported for $LiNiO_2$ [19], and the decrease in charge-transfer impedance was also attributed to expansion of the interlayer distance between NiO_2. Fig. 6(b) shows the dependence of C_{sl} and C_{dl} as a function of charge voltage. The surface layer capacitance increases with increase in charge voltage. Since $C_{sl} = S$ (surface layer area)/ℓ (surface layer thickness), it is obvious that the increase in the surface layer area is larger than that in the surface layer thickness (surface layer resistance). This may be attributed to migration of transition metal atoms into the Li layer, as discussed above for XRD data. On the other hand, the double-layer capacitance also increases with increase in charge voltage. This observation reinforces the above result that the effective surface area increases with charging.

Nyquist plots of a $Li_{1.27}Cr_{0.2}Mn_{0.53}O_2$ electrode obtained at different states of discharge are given in Fig. 7. The size of the semicircle increases slowly above 3.5 V and, thereafter, it increases monotonically with decrease in the discharge potential. The data were further analyzed with the equivalent circuit in Fig. 5. Fig. 8(a) shows the dependence of both surface-layer resistance and charge-transfer resistance as a function of discharge potential. The former parameter increases slowly with decrease in discharge voltage, which indicates slow growth of the passive film with time. The charge-transfer resistance increases slowly with decrease in discharge voltage. The lower the potential and the more the lithium is inserted, the charge-transfer resistance increases monotonically. Fig. 8(b) shows the dependence of C_{sl} and C_{dl} values as a function of discharge potential. The surface-layer capacitance decreases with

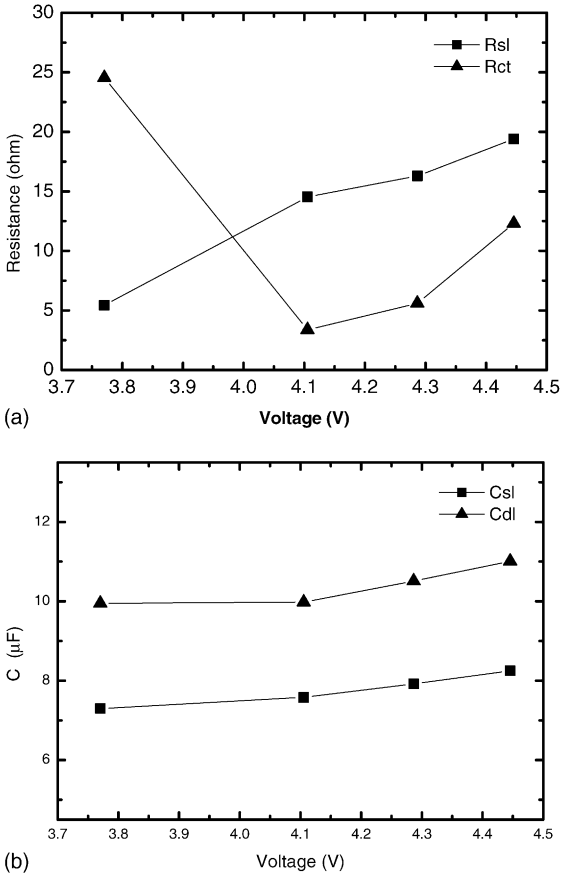

Fig. 6. For $Li_{1.27}Cr_{0.2}Mn_{0.53}O_2$ electrode: (a) variation of surface-layer resistance (R_{sl}) and charge-transfer resistance (R_{ct}) as function of charge voltage; (b) variation of surface-layer capacitance (C_{sl}) and double-layer capacitance (C_{dl}) as function of charge voltage.

decrease in voltage due to the increase in surface-1ayer thickness (surface-layer resistance) On the other hand, the double-layer capacitance remains almost constant with increase in discharge voltage. This suggests that the effective surface area of the electrode does not increase with time

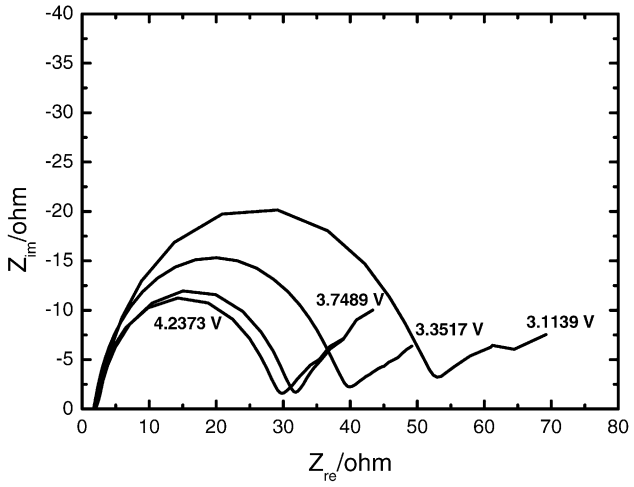

Fig. 7. Nyquist plots for $Li_{1.27}Cr_{0.2}Mn_{0.53}O_2$ electrode measured at different states of discharge.

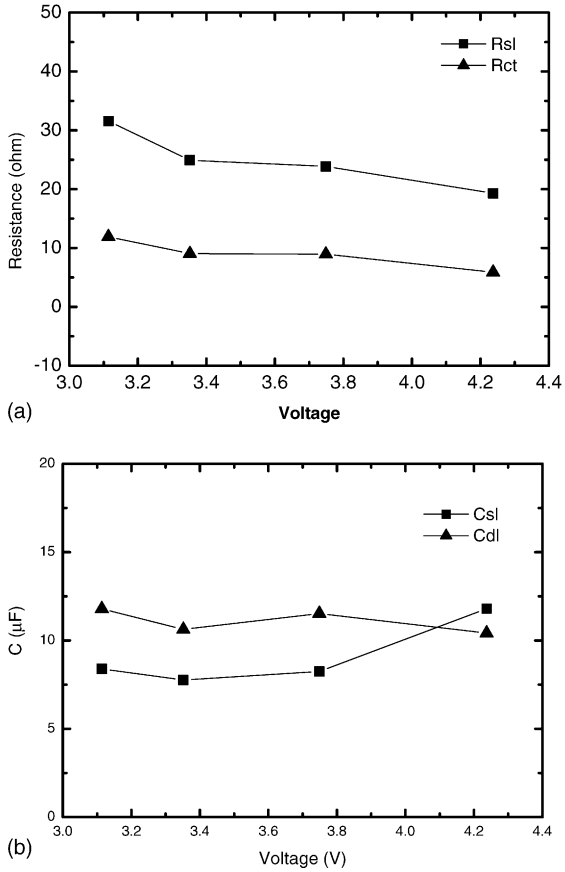

Fig. 8. For $Li_{1.27}Cr_{0.2}Mn_{0.53}O_2$ electrode: (a) variation of surface-layer resistance (R_{sl}) and charge-transfer resistance (R_{ct}) as function of discharge voltage; (b) variation of surface-layer capacitance (C_{sl}) and double-layer capacitance (C_{dl}) as a function of discharge voltage.

during discharge [13]. The result further confirms that the structural change of the $Li_{1.27}Cr_{0.2}Mn_{0.53}O_2$ electrode mainly occurs during the charging process.

Nyquist plots of a $Li_{1.27}Cr_{0.2}Mn_{0.53}O_2$ pristine electrode and those measured after 1, 30 and 40 cycles are shown in Fig. 9. It is clear that the semicircle decreases significantly

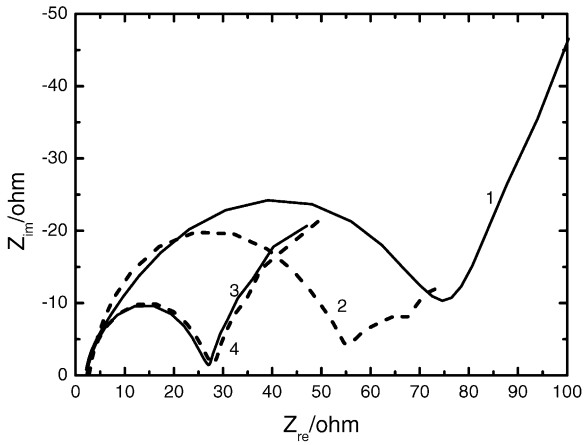

Fig. 9. Nyquist plots for $Li_{1.27}Cr_{0.2}Mn_{0.53}O_2$ electrode obtained at 3.2 V: (1) pristine, (2) after first cycle, (3) after 30th cycle, (4) after 40th cycle.

in size up to the 30th cycle. This indicates that the charge-transfer resistance decreases in the first 30 cycles and thus speeds up the kinetics of the intercalation–deintercalation processes. This may be due to some reorganization of the active mass structure that occurs during the cycling process, as shown in Fig. 4. Upon further cycling, the spectrum is nearly unchanged, which suggests that the electrode is stable after 30 cycles. On the other hand, the sloping line of the pristine electrode display pronounced deviation from a typical Warburg impedance, i.e. it is highly resistive.

4. Conclusions

To explain the capacity increase on extended cycling, $Li_{1.27}Cr_{0.2}Mn_{0.53}O_2$ electrodes with α-$NaFeO_2$ structure have been investigated by means of various electroanalytical techniques and ex situ XRD. Cyclic voltammetry reveals that $Li_{1.27}Cr_{0.2}Mn_{0.53}O_2$ material does not transform into a spinel structure with cycling. The XRD data further reveal that partially-irreversible transition metal atoms (Cr or Mn) accumulate in both the tetrahedral interstitial and the octahedral sites in the lithium layer with cycling, and eventually result in a monoclinic phase and capacity increase. The strong response of impedance spectra also suggests that the structural change occurs mainly during the charging process.

Acknowledgements

This work has been supported by funds from the Korean Ministry of Information and Communication (MIC No. 2003-S-003).

References

[1] C. Storey, I. Kargia, Y. Grincourt, I.J. Davidson, Y.C. Yoo, D.Y. Seung, J. Power Sources 97–98 (2001) 541.
[2] Z.P. Guo, S. Zhong, G.X. Wang, G. Walter, H.K. Liu, S.X. Dou, J. Electrochem. Soc. 149 (2002) A792.
[3] B. Ammudsen, J. Paulsen, I. Davidson, R. Liu, C. Shen, J. Chen, L. Jang, J. Lee, J. Electrochem. Soc. 149 (2002) A431.
[4] Z. Lu, J.R. Dahn, J. Electrochem. Soc. 149 (2002) A1454.
[5] S.T. Myung, S. Komaba, N. Hirosaki, N. Kumagai, K. Arai, R. Kodama, Y. Terada, I. Nakai, Abstract No. 90, The 11th International Meeting on Lithium Batteries, Monterey, USA, June 23–28, 2002.
[6] M. Balasubramanian, J. McBreen, I.J. Davidson, P.S. Whitfiled, I. Kargina, J. Electrochem. Soc. 149 (2002) A176.
[7] Z. Lu, J.R. Dahn, J. Electrochem. Soc. 150 (2003) A1044.
[8] X. Wu, K.S. Ryu, Y.-S. Hong, Y.J. Park, S.H. Chang, J. Power Sources 132 (2004) 219.
[9] S.-H. Kang, K. Amine, J. Power Sources 124 (2003) 533.
[10] R. Premanand, A. Durairajan, B. Haran, R. White, B. Popov, J. Electrochem. Soc. 149 (2002) A54.
[11] D. Aurbach, M.D. Levi, E. Levi, H. Teller, B. Markovsky, G. Salitra, U. Heider, L. Heider, J. Electrochem. Soc. 145 (1998) 3024.
[12] S. Kang, J.B. Goodenough, Electrochem. Solid-Sate Lett. 3 (2000) A536.

[13] D. Zhang, B.N. Popov, R.E. White, J. Power Sources 76 (1998) 81.
[14] X. Wu, S.B. Kim, J. Power Sources 109 (2002) 53.
[15] K.M. Shaju, G.V. Subbarao, B.V.R. Chowdari, J. Electrochem. Soc. 150 (2003) A1.
[16] P. Arora, B.N. Popov, R.E. White, J. Electrochem. Soc. 145 (1998) 807.
[17] X. Wu, Y. Park, K.S. Ryu, Y. Lee, S.H. Chang, Solid State Ionics 169 (2004) 145.
[18] A. Kajiyama, K. Takada, K. Arihara, T. Inada, H. Sasaki, S. Kondo, M. Watanabe, J. Electrochem. Soc. 150 (2003) A157.
[19] S. Yamada, M. Fujuwara, M. Kanda, J. Power Sources 54 (1995) 209.